ACS APPLIED MATERIALS & INTERFACES

Research Article

www.acsami.org

Trimetallic PtSnRh Wavy Nanowires as Efficient Nanoelectrocatalysts for Alcohol Electrooxidation

Kezhu Jiang,[†] Lingzheng Bu,[†] Pengtang Wang,[†] Shaojun Guo,*[,‡] and Xiaoqing Huang*[,†]

[†]College of Chemistry, Chemical Engineering and Materials Science, Soochow University, Suzhou, Jiangsu 215123, China

[‡]Physical Chemistry and Applied Spectroscopy, Los Alamos National Laboratory, Los Alamos, New Mexico 87545, United States

Supporting Information

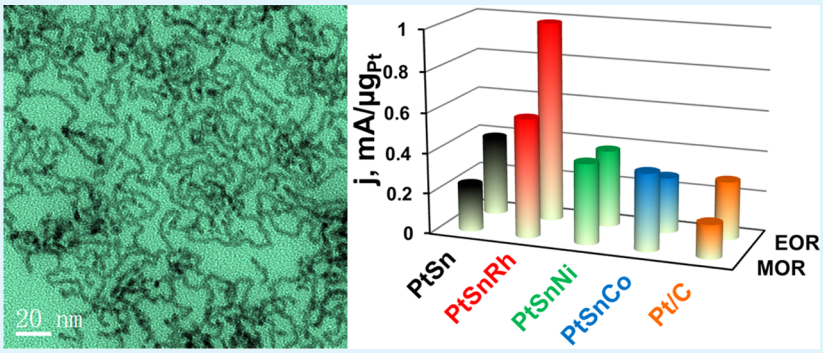

ABSTRACT: The design and creation of efficient catalysts for alcohol oxidation reaction has attracted great research attention because alcohols are promising fuels for direct fuel cell reactions because of their high energy density, easy storage, and transportation. We herein report an efficient strategy that allows the preparation of ternary PtSnM (M = Co, Ni, and Rh) wavy nanowires (WNWs) with ultrathin diameter of only around 2 nm and tunable compositions in high yield. Detailed catalytic studies show that all the ternary WNWs exhibit high performance for ethanol oxidation reaction (EOR) and methanol oxidation reaction (MOR), and their performance shows interesting composition-dependent electrocatalytic activity with PtSnRh WNWs having the best activity for both EOR and MOR. The PtSnRh WNWs are also more stable than commercial Pt/C catalyst, as revealed by long-time chronoamperometric (CA) measurements. The present work highlights the use of multimetallic WNWs as highly active and durable nanocatalysts in enhancing alcohol electrooxidation, which will open a new way in tuning 1D multimetallic nanostructures for boosting other fuel cell reactions, various heterogeneous reactions, and beyond.

KEYWORDS: *platinum, tin, rhodium, wavy nanowires, alcohol electrooxidation*

INTRODUCTION

Direct alcohols fuel cells are considered to be one of the most promising clean energy sources with high energy conversion efficiency, high energy density, easy storage and transportation, and low environmental pollution.[1−3] However, the commercialization of the direct alcohol fuel cell technology has been hindered by the sluggish ethanol oxidation reaction (EOR) or methanol oxidation reaction (MOR) at the anode largely because of the lack of highly active anodic catalysts.[4−6] Compared to methanol, ethanol has higher energy density because of the nature of 12 electron transfer upon complete oxidation, but it is more difficult for complete oxidation via C−C bond cleavage.[2,7] Therefore, design and creation of highly active catalysts for EOR is highly desirable and a great challenge. Nanostructured Pt is the most common catalyst for EOR.[8,9] However, the issues of limited resources, high price, and low tolerance to poisoning heavily limit Pt catalyst application.[10−12] Recent research has focused on the development of multicomponent metal catalysts to modify the Pt electronic structure and to improve the Pt catalytic efficiency.[4] Indeed, the combination of non-noble metals with Pt has provided an effective pathway to reduce the overall usage of expensive Pt and to address the problem of poisoning. This has been well demonstrated in alloying Pt with a second metal Ru, facilitating the formation of adsorbed OH species, for promoting the oxidation of poisoning intermediates.[7,13] The bimetallic Pt-based catalysts show considerable improvements of activity, but they are still very limited efficient catalysts for EOR.[14] Recently, ternary nanoparticle electrocatalysts show the enhanced electrocatalytic activity toward EOR compared with their binary counterparts.[2,15] Apart from the composition, the geometry of catalysts directly associated with the surface atomic arrangement can also be tuned for electrocatalysis optimization. Unfortunately, the majority of previous reported ternary Pt-based nanostructures are mainly polyhedral nanocrystals,

Received: May 21, 2015
Accepted: June 22, 2015
Published: June 22, 2015

DOI: 10.1021/acsami.5b04391
ACS Appl. Mater. Interfaces 2015, 7, 15061−15067

usually showing good activity but very limited stability for EOR.[16−19]

Among various nanostructures, nanowires (NWs) are found to be more promising in catalysis.[20−29] In general, the NWs can contact with the carbon support more effectively than the polyhedral nanocrystals. This will not only enhance the electron transfer between NWs and carbon support more effectively but also prevent the aggregation, coalescence, and Ostwald ripening of NWs.[20] Furthermore, when the diameter of the NWs is reduced to less than 3 nm, they can exhibit attractive characteristics of size effect, which can further enhance the electrocatalytic activity.[30,31] For example, it was demonstrated that the Pt alloy ultrathin NWs with diameter of around 2.5 nm have exhibited excellent activity and stability in both anodic and cathodic fuel cell reactions.[24,32,33] Therefore, combination of the advantages from the ultrathin NWs and the effects of ternary metal nanostructures can make further improvements in both activity and durability for different catalytic reactions.

Herein, we report our efforts on the controlled production of ternary PtSnRh wavy nanowires (WNWs) with ultrathin feature. The key part for our synthesis for multimetallic NWs is its robust approach to produce different types of ternary WNWs, including PtSnNi WNWs and PtSnCo WNWs. These ternary WNWs show interesting composition-dependent electrocatalytic activity for both EOR and MOR with PtSnRh WNWs having the best activity. The PtSnRh WNWs are also more stable than commercial Pt/C catalyst. The present work opens a new way to design different types of multimetallic NWs for optimizing the electrocatalytic performance for the alcohol electrooxidation reaction.

EXPERIMENTAL SECTION

Chemicals. Platinum(II) acetylacetonate ($Pt(acac)_2$, 97%), rhodium(III) acetylacetonate ($Rh(acac)_3$, 97%), nickel(II) acetylacetonate ($Ni(acac)_2$, 97%), cobalt(II) acetylacetonate ($Co(acac)_2$, 97%), tin(II) chloride ($SnCl_2$, ≥99%), oleic acid ($CH_3(CH_2)_7CH{=}CH(CH_2)_7COOH$, OAc, ≥99%) and oleylamine ($CH_3(CH_2)_7CH{=}CH(CH_2)_7CH_2NH_2$, OA, 68−70%), and ascorbic acid ($C_6H_8O_6$, AA, reagent grade) were all purchased from Sigma-Aldrich. All the chemicals were used as received without further purification. The deionized water used in all experiments was prepared by passing through an ultrapure purification system (Aqua Solutions).

Preparation of PtSnRh, PtSnNi, PtSnCo, and PtSn Wavy Nanowires (WNWs). In a typical preparation of PtSnRh WNWs, $Pt(acac)_2$ (10.0 mg), $SnCl_2$ (15 mg), $Rh(acac)_3$ (3.3 mg), AA (35.6 mg), 4 mL OA, and 1 mL OAc were placed into a vial (volume: 30 mL). After the vial had been capped, the mixture was ultrasonicated for around 60 min. The resulting homogeneous mixture was then heated at 190 °C for 10 h in an oil bath before it was cooled to room temperature. The resulting colloidal products were collected by centrifugation and were washed three times with an ethanol (8 mL) + cyclohexane (1 mL) mixture. The synthetic procedures for PtSnNi, PtSnCo, and PtSn WNWs were the same as that of PtSnRh WNWs except for changing $Rh(acac)_3$ with $Ni(acac)_2$ or $Co(acac)_2$ or for the absence of $Rh(acac)_3$, respectively. PtSnRh WNWs with different Rh contents were prepared by keeping the same amount of the $Pt(acac)_2$ (10.0 mg) and $SnCl_2$ (15 mg) while using a different amount of the $Rh(acac)_3$. The samples obtained by using 1.1, 2.2, 3.3, and 4.4 mg of $Rh(acac)_3$ were denoted as PtSnRh-1, PtSnRh-2, PtSnPh-3, and PtSnRh-4, respectively.

Catalyst Preparation. Different types of WNWs and VC-X72 carbon were mixed in a 20 mL ethanol/cyclohexane mixture (V/V = 1/1) and were subjected to sonication for 60 min to deposit WNWs on carbon. The catalysts were separated by centrifugation and were washed with the ethanol/cyclohexane mixture three times.

Characterizations. Transmission electron microscopy (TEM) and scanning transmission electron microscopy (STEM) were conducted on an FEI Tecnai F20 transmission electron microscope at an acceleration voltage of 200 kV. Scanning electron microscopy (SEM) images were taken with a Zeiss scanning electron microscope. The samples were prepared by dropping a cyclohexane dispersion of samples onto carbon-coated copper TEM grids using pipettes and by drying under ambient condition. Powder X-ray diffraction (XRD) patterns were collected on a Shimadzu XRD-6000 X-ray diffractometer. The concentration of catalysts was determined by the inductively coupled plasma atomic emission spectroscopy (710-ES, Varian, ICP-AES). X-ray photoelectron spectroscopy (XPS) tests were done with an SSI S-Probe XPS Spectrometer. The carbon peak at 285.0 eV was used as a reference to correct for charging effects.

Ethanol and Methanol Electrooxidation Measurements. A three-electrode cell was used to do the electrochemical measurements. The working electrode was a glassy-carbon rotating disk electrode (RDE) (diameter: 5 mm, area: 0.196 cm^2) from Pine Instruments. A saturated calomel electrode (SCE) and a platinum wire were used as the reference electrode and counter electrode, respectively. The catalyst ink was prepared by ultrasonically mixing 3 mg of catalysts with 780 μL of isopropyl alcohol, 200 μL of water, and 20 μL of 5 wt % Nafion solution for 1 h. Ten microliters of the suspension was deposited on a glassy carbon electrode to obtain the working electrodes after the solvent dried naturally. The potential scan rate was 50 mV/s for the cyclic voltammetry (CV) measurements. Ethanol electrooxidation measurements were conducted in a 0.1 M NaOH and 0.1 M ethanol solution. The chronoamperometric (CA) measurement of ethanol electrooxidation were held at −0.25 V for 5000 s in the same solution. Methanol electrooxidation measurements were conducted in a 0.1 M NaOH and 0.1 M methanol solution. The CA measurement of methanol electrooxidation was held at −0.3 V for 5000 s in the same solution. For comparison, commercial Pt/C (Aldrich, 80980-5G) was used as the baseline catalyst, and the same procedure as described above was used to conduct the electrochemical measurement. The Pt loadings of all catalysts were 3.0 μg. All electrochemical experiments were performed at room temperature.

RESULTS AND DISCUSSION

The ultrathin PtSnRh WNWs were typically produced by simultaneous reduction of platinum(II) acetylacetonate ([$Pt(acac)_2$]), rhodium(III) acetylacetonate ([$Rh(acac)_3$]), and tin(II) chloride ($SnCl_2$) by the use of oleylamine/oleic acid mixture as solvent and surfactant and by the use of ascorbic acid (AA) as the reducing agent (see Experimental section for details). The morphology and structure of the as-prepared PtSnRh WNWs are initially characterized by transmission electron microscopy (TEM). The representative TEM images reveal that the products consist of NWs with high yield (Figure 1a and Figure S1 of the Supporting Information). These

DOI: 10.1021/acsami.5b04391
ACS Appl. Mater. Interfaces 2015, 7, 15061−15067

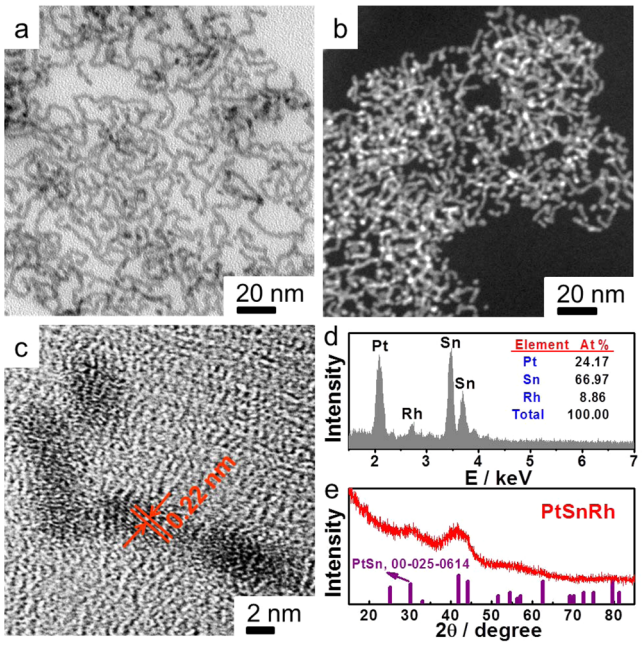

Figure 1. Morphological and structural analyses for ultrathin ternary PtSnRh WNWs. Representative (a) TEM image, (b) HAADF-STEM image, (c) HRTEM image, (d) EDX pattern, and (e) XRD pattern of the ultrathin ternary PtSnRh WNWs.

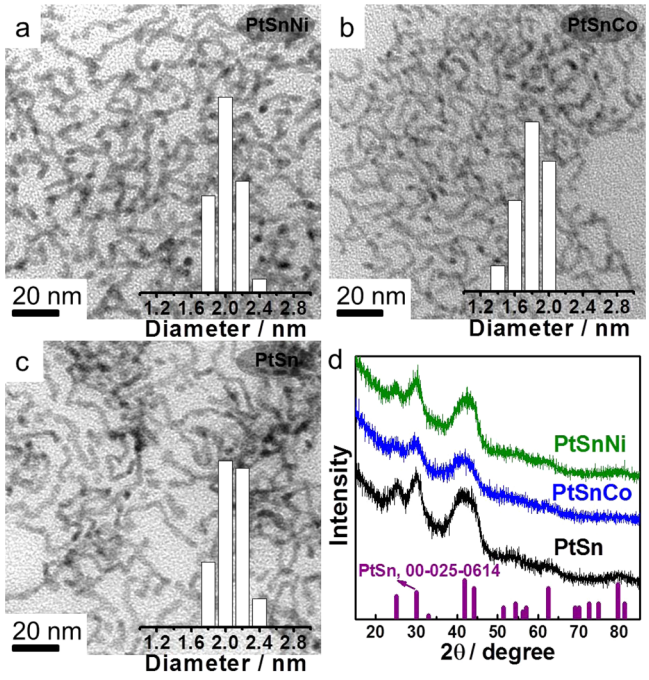

Figure 2. Representative TEM images of (a) PtSnNi WNWs, (b) PtSnCo WNWs, and (c) PtSn WNWs. The inset: the relative diameter histogram of PtSnNi WNWs, PtSnCo WNWs, and PtSn WNWs. (d) XRD patterns of PtSnNi WNWs, PtSnCo WNWs, and PtSn WNWs.

WNWs are frequently bent on the TEM grid, suggesting their highly flexible nature. All the surveyed NWs show a wavelike profile. The wavy character of the NWs is further visualized by high-angle annular dark-field scanning TEM (HAADF-TEM) (Figure 1b and Figure S1c of the Supporting Information). The products are unique with the length in the range of tens of nanometers and the average diameter of 2.2 nm as determined by manually measuring 100 randomly selected wires (Figure S1d of the Supporting Information). The high-resolution TEM (HRTEM) image of a single WNW (Figure 1c) shows that the interplanar spacing is measured as 0.22 nm, assigned to the (102) plane of the hexagonal PtSn intermetallic nanostructure.[34] The energy-dispersive X-ray spectrum (EDX) (Figure 1d) reveals that the sample is mainly composed of Pt, Sn, and Rh elements in the WNWs. The atomic ratio of Pt/Sn/Rh is determined to be 1:2.7:0.37, as presented in the inset of Figure 1d. This result is in accordance with the inductively coupled plasma optical emission spectrometer (ICP-AES) result. The powder X-ray diffraction (XRD) pattern of the PtSnRh WNWs displays the hexagonal pattern associated with the PtSn intermetallic nanostructure (JCPDS No. 00-25-0614). The broadened diffraction peaks from WNWs reveal the small dimension of the crystal domains, further confirming the ultrathin feature of these PtSnRh WNWs.[25,35]

Significantly, the synthesis approach for ultrathin ternary PtSnRh WNWs can be extended to the synthesis of other ternary WNWs, such as PtSnNi WNWs and PtSnCo WNWs. The PtSnNi WNWs and PtSnCo WNWs were readily obtained by changing $Rh(acac)_3$ with $Ni(acac)_2$ or $Co(acac)_2$, respectively. Figure 2a–c shows the typical TEM images of PtSnNi WNWs, PtSnCo WNWs, and PtSn WNWs, respectively. The corresponding diameter histograms of PtSnNi WNWs, PtSnCo WNWs, and PtSn WNWs are shown in the insets of Figure 2a–c. The TEM image taken from PtSnNi WNWs reveals the formation of one-dimensional wavelike nanostructures, similar to that of PtSnRh WNWs (Figure 2a). The average diameter of these NWs is measured to be 1.9 nm. The Pt/Sn/Ni atomic ratio is close to 1:2.9:0.35, confirmed by both the EDX analysis (Figure S2 of the Supporting Information) and the ICP-AES result. The TEM image in Figure 2b shows the PtSnCo WNWs with an average diameter of 1.8 nm. The EDX result indicates that Pt, Sn, and Co elements have the atomic ratio of about 1:2.6:0.34 (Figure S3 of the Supporting Information). Figure 2c shows the TEM image of PtSn WNWs with an average diameter of 2.0 nm. The corresponding EDX result indicates that the atomic ratio of Pt/Sn of PtSn WNWs is close to 1:3 (Figure S4 of the Supporting Information). Therefore, all the characterizations collectively confirm the successful production of ultrathin PtSnNi, PtSnCo, and PtSn WNWs. The XRD patterns of all the WNWs are shown in Figure 2d. It is clear that all the WNWs show the typical diffraction peaks of PtSn, and no other detectable peaks are observed in the XRD patterns. It can be also seen that the width of the main peaks are close to each other, indicating the similar sizes of these WNWs.

The surface properties of these WNWs were measured by X-ray photoelectron spectroscopy (XPS). The Pt 4f, Sn 3d, Rh 3d, Co 2p, and Ni 2p peaks of different samples are summarized in Figure 3. A representative high-resolution Pt 4f spectrum of PtSnRh, PtSnNi, PtSnCo, and PtSn WNWs is shown in Figure 3a. It is clear that the majority of the Pt in these WNWs is mainly in the metallic state (Table S1 of the Supporting Information). Compared with bimetallic PtSn WNWs, a slight shift of the Pt 4f2/7 peak toward lower values is observed for the ternary PtSnRh WNWs, PtSnNi WNWs, and PtSnCo WNWs. The slight shift of the Pt 4f2/7 peak indicates the changes of the electronic structure of Pt when the third element is added into PtSn WNWs.[36,37] The lowest value of the Pt 4f2/7 peak of PtSnRh WNWs indicates the biggest

DOI: 10.1021/acsami.5b04391
ACS Appl. Mater. Interfaces 2015, 7, 15061–15067

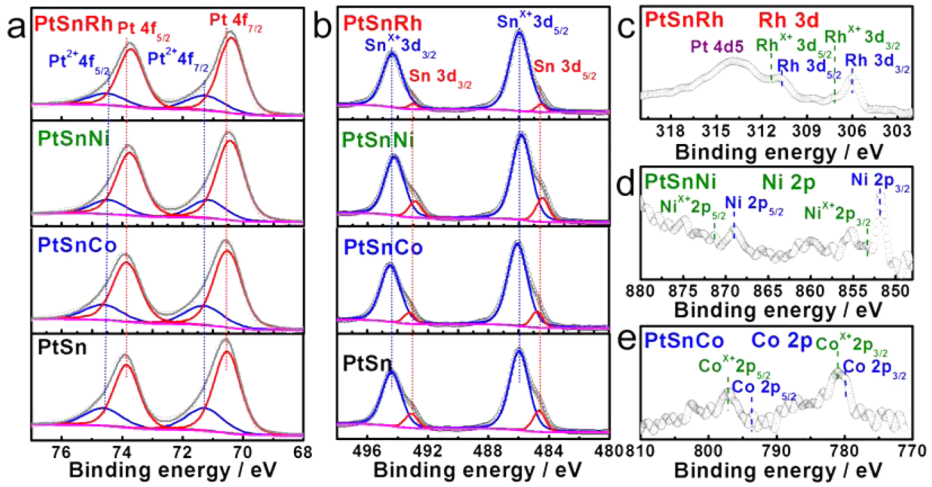

Figure 3. XPS patterns of PtSnRh, PtSnRhNi, PtSnRhCo, and PtSn WNWs. (a) Pt 4f and (b) Sn 3d. (c) Rh 3d of PtSnRh WNWs, (d) Ni 2p of PtSnNi WNWs, and (e) Co 2p of PtSnCo WNWs.

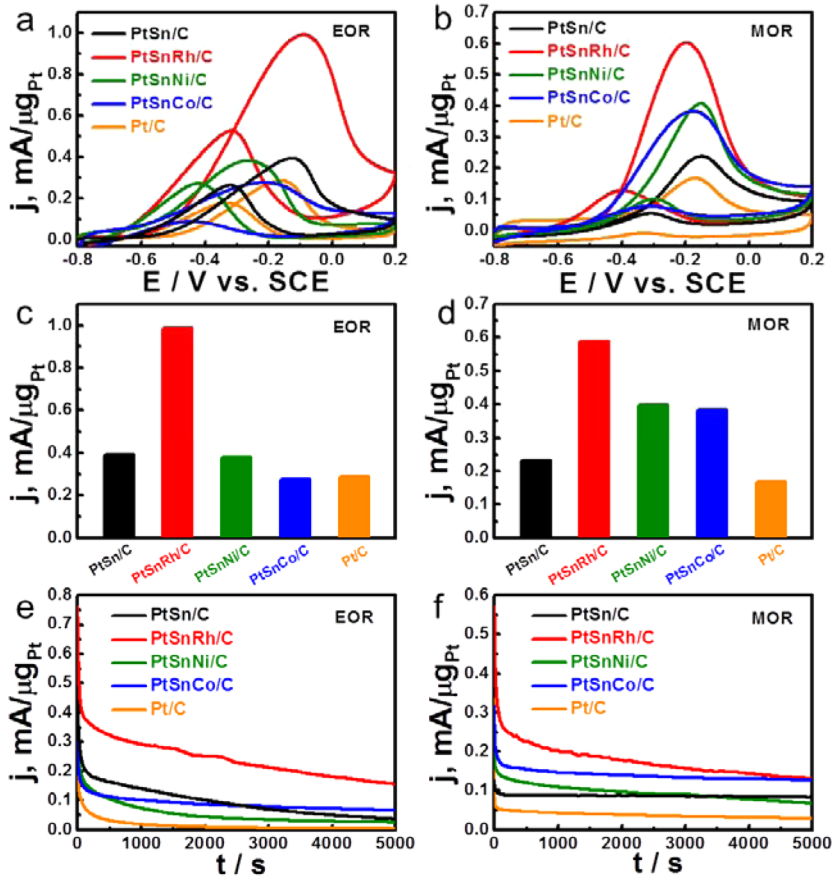

Figure 4. (a) CVs of PtSn/C, PtSnRh/C, PtSnNi/C, PtSnCo/C, and Pt/C in a solution containing 0.1 M NaOH + 0.1 M ethanol. (b) CVs of different catalysts in 0.1 M NaOH + 0.1 M methanol. (c) Summary of peak current density of different catalysts for EOR. (d) Summary of peak current density of different catalysts for MOR. (e) Current−time curves of different catalysts recorded at −0.25 V toward EOR. (f) Current−time curves of different catalysts recorded at −0.2 V toward MOR.

change in the electronic structure of Pt when it is added with Rh. The majority of Sn in these WNWs is oxidized (Figure 3b, Table S1 of the Supporting Information). The small peaks of these WNWs at about 484.5 eV indicate the presence of metallic Sn in the WNWs.[38] The representative high-resolution spectra of Rh 3d, Co 2p, and Ni 2p are given in Figure 3c−e, respectively. The peaks of these elements confirm that these elements do exist in the produced NWs. Rh 3d5/2 spectra at ∼306 eV suggest the presence of metallic Rh. The XPS results suggest that the most possible scheme is the formation of the Pt−Sn−Rh alloy in PtSnRh WNWs consistent with the XRD results.[36] Therefore, it can be concluded that the active surface of the PtRhSn WNWs evolved into active catalytic sites characterized by uniformly distributed metallic Pt, Sn, and Rh

DOI: 10.1021/acsami.5b04391
ACS Appl. Mater. Interfaces 2015, 7, 15061−15067

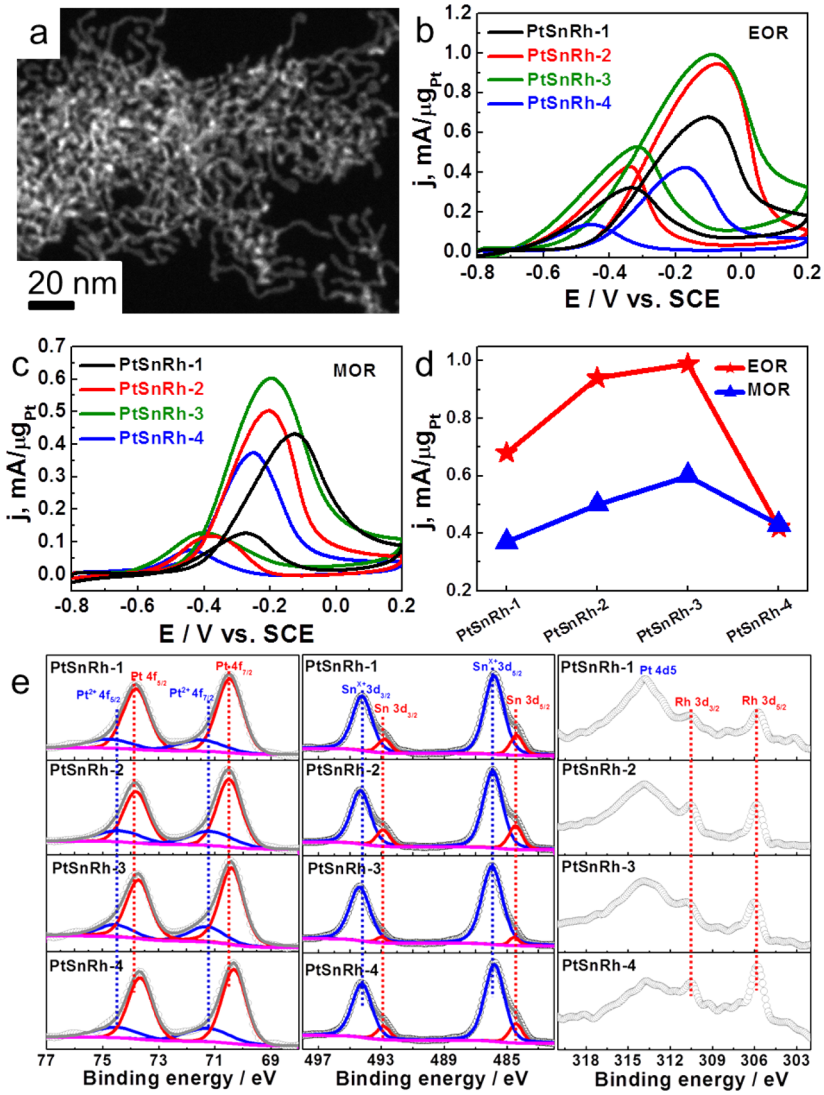

Figure 5. (a) Representative HAADF-STEM image of PtSnRh-4. CVs of PtSnRh-1 WNWs, PtSnRh-2 WNWs, PtSnRh-3 WNWs, and PtSnRh-4 WNWs (b) in 0.1 M NaOH + 0.1 M ethanol and (c) in 0.1 M NaOH + 0.1 M methanol. (d) Summary of peak current density of PtSnRh WNWs with different atomic ratios of Rh/Pt for EOR and MOR. (e) Pt 4f, Sn 3d, and Rh 3d XPS patterns of PtSnRh-1, PtSnRh-2, PtSnRh-3, and PtSnRh-4 WNWs.

surface sites in atomic neighborhood to oxophilic surface SnOx.[36]

These ultrathin ternary WNWs were loaded onto a carbon support (Vulcan XC-72) for further characterization of electrochemical properties. Studies of alkaline fuel cells have received much attention in recent years as an alternative to common acid fuel cells. One of the most important advantages lies in the fact that the reaction kinetics in alkaline solution is higher than that in acid medium.[39] To this end, we studied the performance of our ultrathin ternary WNWs as catalysts for both the methanol and the ethanol electrooxidation in the alkaline solution. Figure S5a of the Supporting Information is the typical TEM image of the PtSnRh WNWs loaded on the carbon. The WNWs/C were dispersed in deionized water + isopropanol + 5 wt % nafion (V:V:V 1:4:0.01). Next, 10 μL of this dispersion was deposited on the surface of glassy carbon electrode, and the WNWs were fixed onto the electrode by Nafion once the solvent was evaporated. The commercial Pt/C catalyst was used as the reference (Figure S6a of the Supporting Information). The Pt mass loadings of WNWs/C and commercial Pt/C catalysts were all fixed at 3 μg. Electrooxidation toward ethanol was carried out in an aqueous solution containing 0.1 M NaOH and 0.1 M ethanol, using a cyclic voltammetry measurement technique, sweeping from −0.8 to 0.2 V (vs SCE) at a scan rate of 50 mV/s. Figure 4a shows the mass activity for PtSn, PtSnRh, PtSnNi, PtSnCo, and Pt/C catalysts toward ethanol electrooxidation. The onset potential of PtSnRh WNWs, PtSnNi WNWs, and PtSnCo WNWs is lower than that of the PtSn WNWs and the commercial Pt/C catalyst, indicating the enhancement in the kinetics of the ethanol oxidation reaction by the ternary WNWs. Among four kinds of WNWs investigated, PtSnRh WNWs show the highest peak current density at 0.99 mA/μg_{Pt}, which is 3.4 times higher than that of the Pt/C catalyst (0.29 mA/μg_{Pt}) and 2.5 times higher than that of the PtSn WNWs (0.39 mA/μg_{Pt}) (Figure 4c). The high activity of PtSnRh WNWs can be attributed to promoting the C−C bond cleavage by the existence of Rh;[2] the synergistic effect between Pt, Rh, and Sn;[40,41] and the wavy nanostructure with ultrathin size.[30,34,42] Furthermore, the close interaction of the Pt/Rh/

DOI: 10.1021/acsami.5b04391
ACS Appl. Mater. Interfaces 2015, 7, 15061−15067

Sn and SnOx moieties may also be instrumental in the high electrocatalytic activity performance.[2,36] The stability of these WNWs toward ethanol electrooxidation is investigated by a CA measurement technique, carried out at −0.25 V (vs SCE) for 5000 s in a solution containing 0.1 M NaOH and 0.1 M ethanol (Figure 4e). We found that the current decay for the reaction on the PtSnRh WNWs is significantly slower than that on the commercial Pt/C catalyst and other WNWs, indicating their better tolerance toward ethanol electrocatalysts. After 5000 s, the residue current of PtSnRh WNWs is also much higher than that of commercial Pt/C and all the other WNWs. The catalysts were collected by sonicating the glassy carbon disk electrode in ethanol after the CA measurement, and their structures were observed by TEM (Figures S5b and S6b of the Supporting Information). The Pt/C catalyst shows an increase in nanoparticle size from ∼2 to ∼10 nm after the CA measurement (Figure S6b of the Supporting Information). In contrast, the PtSnRh/C catalyst displays similar features before and after the CA measurement with wavy-like nanostructure and ultrathin diameter distribution (Figure S5b of the Supporting Information). The ultrathin ternary WNWs are also active catalysts for MOR. Figure 4b, d, and f summarizes the CV curves, the peak mass activities, and the CA measurement results of MOR, respectively. Among all the WNWs studied, the PtSnRh WNWs also show the highest catalytic activity (Figure 4b and d). The peak current density of the PtSnRh WNWs is calculated to be 0.6 mA/μg_{pt}, which is 3.5 times higher than that of Pt/C. After 5000 s CA measurement, the catalytic activity of the PtSnRh WNWs, PtSnNi WNWs, PtSnCo, and PtSn WNWs are still much higher than that of Pt/C (Figure 4f). The high activity of PtSnRh WNWs for MOR can be ascribed to the strong interactions between Pt and Rh and to the largest change of electronic structure of Pt when it is added with Rh, as indicated by XPS analyses (Figure 3).

To further optimize the performance of PtSnRh WNWs, three other PtSnRh WNWs with different contents of Rh were prepared by slightly changing the amount of $Rh(acac)_3$ precursor supplied from 1.1 to 4.4 mg while keeping the amount of the Pt precursor at 10 mg and the Sn precursor at 15 mg. The obtained samples prepared with $Rh(acac)_3$ precursor supplied of 1.1, 2.2, 3.3, and 4.4 mg are denoted as PtSnRh-1, PtSnRh-2, PtSnPh-3, and PtSnRh-4, respectively. Figures S7a, S8a, and S9a of the Supporting Information show typical TEM images of the as-prepared PtSnRh-1, PtSnRh-2, and PtSnRh-4 WNWs. It is clear that these three samples also show the similar wavy nanostructure. The average diameters of these WNWs are measured to be 1.9, 1.9, and 2.1 nm for PtSnRh-1, PtSnRh-2, and PtSnRh-4 WNWs, respectively (Figures S7b, S8b, and S9b of the Supporting Information). The PtSnRh-4 WNWs are selectively characterized by the HAADF-STEM image (Figure 5a, Figure S10a of the Supporting Information) and the HRTEM image (Figure S10b of the Supporting Information). The successful formation of ternary PtSnRh WNWs is further confirmed by ICP-AES, EDX (Figures S11b, S12b, and S13b of the Supporting Information), and XPS (Figure 5e). It is clear that the peak intensity of Pt 4d5/2 decreases and that the peak intensity of Rh 3d5/2 increases, with the increase of the Rh/Pt atomic ratio, which is in accordance with the EDX results. The corresponding XRD results are similar to each other, associated with the PtSn intermetallic nanostructure (Figure S14 of the Supporting Information). The electrocatalytic activities of PtSnRh WNWs with different Rh contents were further examined. Figure 5b and c shows the electrochemistry property of these WNWs toward EOR and MOR. The Pt−Rh composition effect is clearly observed. The summary of peak current density of different samples for EOR and MOR is shown in Figure 5d. Similar trends are obtained for both EOR and MOR: the PtSnPh-3 WNWs give the highest peak mass activity, indicating that the proper tuning composition of PtSnRh WNWs is a very important factor for electrocatalysis optimization. The best electrochemical activity of PtSnRh WNWs-3 catalyst is likely because PtSnRh WNWs/C-3 has the highest percentage of Sn^{x+}(Figure 5e, Table S1 of the Supporting Information), which is beneficial for enhancing the electrochemical activity toward alcohol electrooxidation.[36]

CONCLUSIONS

We have successfully synthesized a series of ternary PtSnM (M= Co, Ni, and Rh) WNWs with tunable compositions and ultrathin features. All the ultrathin Pt-based WNWs are active toward both EOR and MOR, and their catalytic activities are highly composition-dependent with PtSnRh WNWs showing the best activity. The performance of the ultrathin PtSnRh WNWs largely outperforms that of the commercial Pt/C catalyst. We expect our fundamental study will inspire rational design of Pt-based multimetallic NWs for various chemical reactions with greatly improved performance but with low Pt usages.

ASSOCIATED CONTENT

Supporting Information

Details of TEM images, HAADF-STEM images, HRTEM images, SEM-EDX patterns, XPS patterns, and XRD patterns for different PtSnM (M = Rh, Co, or Ni) WNWs and commercial Pt/C catalysts. The Supporting Information is available free of charge on the ACS Publications website at DOI: 10.1021/acsami.5b04391.

AUTHOR INFORMATION

Corresponding Authors

*E-mail: hxq006@suda.edu.cn.
*E-mail: shaojun.guo.nano@gmail.com (or sguo@lanl.gov).

Notes

The authors declare no competing financial interest.

ACKNOWLEDGMENTS

This work was financially supported by the start-up funding from Soochow University and Young Thousand Talented Program.

REFERENCES

(1) Tian, N.; Zhou, Z.-Y.; Sun, S.-G.; Ding, Y.; Wang, Z. L. Synthesis of Tetrahexahedral Platinum Nanocrystals with High-index Facets and High Electro-oxidation Activity. *Science* **2007**, *316*, 732−735.
(2) Kowal, A.; Li, M.; Shao, M.; Sasaki, K.; Vukmirovic, M.; Zhang, J.; Marinkovic, N.; Liu, P.; Frenkel, A.; Adzic, R. Ternary Pt/Rh/SnO_2 Electrocatalysts for Oxidizing Ethanol to CO_2. *Nat. Mater.* **2009**, *8*, 325−330.
(3) Zhao, X.; Yin, M.; Ma, L.; Liang, L.; Liu, C.; Liao, J.; Lu, T.; Xing, W. Recent Advances in Catalysts for Direct Methanol Fuel Cells. *Energy Environ. Sci.* **2011**, *4*, 2736−2753.
(4) Chen, A.; Holt-Hindle, P. Platinum-based Nanostructured Materials: Synthesis, Properties, and Applications. *Chem. Rev.* **2010**, *110*, 3767−3804.

DOI: 10.1021/acsami.5b04391
ACS Appl. Mater. Interfaces 2015, 7, 15061−15067

(5) Antolini, E. Catalysts for Direct Ethanol Fuel Cells. *J. Power Sources* **2007**, *170*, 1−12.
(6) Steele, B. C.; Heinzel, A. Materials for Fuel-cell Technologies. *Nature* **2001**, *414*, 345−352.
(7) Fujiwara, N.; Friedrich, K.; Stimming, U. Ethanol Oxidation on PtRu Electrodes Studied by Differential Electrochemical Mass Spectrometry. *J. Electroanal. Chem.* **1999**, *472*, 120−125.
(8) Zhou, W.; Li, W. Z.; Song, S. Q.; Zhou, Z. H.; Jiang, L.; Sun, G.; Xin, Q.; Poulianitis, K.; Kontou, S.; Tsiakaras, P. Bi-and Tri-metallic Pt-based Anode Catalysts for Direct Ethanol Fuel Cells. *J. Power Sources* **2004**, *131*, 217−223.
(9) Shao, Y.; Yin, G.; Gao, Y. Understanding and Approaches for the Durability Issues of Pt-based Catalysts for PEM Fuel Cell. *J. Power Sources* **2007**, *171*, 558−566.
(10) Winter, M.; Brodd, R. J. What are Batteries, Fuel cells, and Supercapacitors? *Chem. Rev.* **2004**, *104*, 4245−4270.
(11) Hitmi, H.; Belgsir, E.; Léger, J.-M.; Lamy, C.; Lezna, R. A Kinetic Analysis of the Electro-oxidation of Ethanol at a Platinum Electrode in Acid Medium. *Electrochim. Acta* **1994**, *39*, 407−415.
(12) Kavanagh, R.; Cao, X. M.; Lin, W. F.; Hardacre, C.; Hu, P. Origin of Low CO_2 Selectivity on Platinum in the Direct Ethanol Fuel Cell. *Angew. Chem, Int. Ed.* **2012**, *51*, 1572−1575.
(13) Camara, G.; Lima, R.; Iwasita, T. Catalysis of Ethanol Electrooxidation by PtRu: the Influence of Catalyst Composition. *Electrochem. Commun.* **2004**, *6*, 812−815.
(14) Vigier, F.; Coutanceau, C.; Hahn, F.; Belgsir, E.; Lamy, C. On the Mechanism of Ethanol Electro-oxidation on Pt and PtSn Catalysts: Electrochemical and in Situ IR Reflectance Spectroscopy Studies. *J. Electroanal. Chem.* **2004**, *563*, 81−89.
(15) Li, M.; Cullen, D. A.; Sasaki, K.; Marinkovic, N. S.; More, K.; Adzic, R. R. Ternary Electrocatalysts for Oxidizing Ethanol to Carbon Dioxide: Making Ir Capable of Splitting C-C bond. *J. Am. Chem. Soc.* **2012**, *135*, 132−141.
(16) Chen, J.; Lim, B.; Lee, E. P.; Xia, Y. Shape-controlled Synthesis of Platinum Nanocrystals for Catalytic and Electrocatalytic Applications. *Nano Today* **2009**, *4*, 81−95.
(17) Porter, N. S.; Wu, H.; Quan, Z.; Fang, J. Shape-control and Electrocatalytic Activity-enhancement of Pt-based Bimetallic Nanocrystals. *Acc. Chem. Res.* **2013**, *46*, 1867−1877.
(18) Huang, X.; Zhao, Z.; Fan, J.; Tan, Y.; Zheng, N. Amine-assisted Synthesis of Concave Polyhedral Platinum Nanocrystals Having {411} High-index Facets. *J. Am. Chem. Soc.* **2011**, *133*, 4718−4721.
(19) Lai, J.; Niu, W.; Luque, R.; Xu, G. Solvothermal Synthesis of Metal Nanocrystals and Their Applications. *Nano Today* **2015**, DOI: 10.1016/j.nantod.2015.03.001.
(20) Koenigsmann, C.; Wong, S. S. One-dimensional Noble Metal Electrocatalysts: a Promising Structural Paradigm for Direct Methanol Fuel Cells. *Energy Environ. Sci.* **2011**, *4*, 1161−1176.
(21) Song, Y.; Garcia, R. M.; Dorin, R. M.; Wang, H.; Qiu, Y.; Coker, E. N.; Steen, W. A.; Miller, J. E.; Shelnutt, J. A. Shelnutt, Synthesis of Platinum Nanowire Networks Using a Soft Template. *Nano Lett.* **2007**, *7*, 3650−3655.
(22) Zhang, L.; Li, N.; Gao, F.; Hou, L.; Xu, Z. J. Insulin Amyloid Fibrils: an Excellent Platform for Controlled Synthesis of Ultrathin Superlong Platinum Nanowires with High Electrocatalytic Activity. *J. Am. Chem. Soc.* **2012**, *134*, 11326−11329.
(23) Ruan, L.; Zhu, E.; Chen, Y.; Lin, Z.; Huang, X.; Duan, X.; Huang, Y. Biomimetic Synthesis of an Ultrathin Platinum Nanowire Network With a High Twin Density for Enhanced Electrocatalytic Activity and Durability. *Angew. Chem, Int. Ed.* **2013**, *52*, 12577−12581.
(24) Guo, S.; Li, D.; Zhu, H.; Zhang, S.; Markovic, N. M.; Stamenkovic, V. R.; Sun, S. FePt and CoPt Nanowires as Efficient Catalysts for the Oxygen Reduction Reaction. *Angew. Chem, Int. Ed.* **2013**, *52*, 3465−3468.
(25) Wang, Y.; Choi, S. I.; Zhao, X.; Xie, S.; Peng, H. C.; Chi, M.; Huang, C. Z.; Xia, Y. Polyol Synthesis of Ultrathin Pd Nanowires via Attachment-based Growth and Their Enhanced Activity towards Formic Acid Oxidation. *Adv. Funct. Mater.* **2014**, *24*, 131−139.
(26) Xia, B. Y.; Wu, H. B.; Yan, Y.; Lou, X. W.; Wang, X. Ultrathin and Ultralong Single-crystal Platinum Nanowire Assemblies with Highly Stable Electrocatalytic Activity. *J. Am. Chem. Soc.* **2013**, *135*, 9480−9485.
(27) Alia, S. M.; Pivovar, B. S.; Yan, Y. Platinum-coated Copper Nanowires with High Activity for Hydrogen Oxidation Reaction in Base. *J. Am. Chem. Soc.* **2013**, *135*, 13473−13478.
(28) Guo, S.; Dong, S.; Wang, E. Pt/Pd Bimetallic Nanotubes with Petal-like Surfaces for Enhanced Catalytic Activity and Stability towards Ethanol Electrooxidation. *Energy Environ. Sci.* **2010**, *3*, 1307−1310.
(29) Liang, H. W.; Cao, X.; Zhou, F.; Cui, C. H.; Zhang, W. J.; Yu, S. H. A Free-Standing Pt-Nanowire Membrane as a Highly Stable Electrocatalyst for the Oxygen Reduction Reaction. *Adv. Mater.* **2011**, *23*, 1467−1471.
(30) Fiorentini, V.; Methfessel, M.; Scheffler, M. Reconstruction Mechanism of *fcc* Transition Metal (001) Surfaces. *Phys. Rev. Lett.* **1993**, *71*, 1051−1054.
(31) Koenigsmann, C.; Zhou, W.-P.; Adzic, R. R.; Sutter, E.; Wong, S. S. Size-dependent Enhancement of Electrocatalytic Performance in Relatively Defect-free, Processed Ultrathin Platinum Nanowires. *Nano Lett.* **2010**, *10*, 2806−2811.
(32) Zhu, H.; Zhang, S.; Guo, S.; Su, D.; Sun, S. Synthetic Control of FePtM Nanorods (M= Cu, Ni) to Enhance the Oxygen Reduction Reaction. *J. Am. Chem. Soc.* **2013**, *135*, 7130−7133.
(33) Guo, S.; Zhang, S.; Sun, X.; Sun, S. Synthesis of Ultrathin FePtPd Nanowires and Their Use as Catalysts for Methanol Oxidation Reaction. *J. Am. Chem. Soc.* **2011**, *133*, 15354−15357.
(34) Ding, J.; Bu, L.; Zhang, N.; Yao, J.; Huang, Y.; Huang, X. Facile Synthesis of Ultrathin Bimetallic PtSn Wavy Nanowires by Nanoparticle Attachment as Enhanced Hydrogenation Catalysts. *Chem.—Eur. J.* **2015**, *21*, 3901−3905.
(35) Yu, X.; Wang, D.; Peng, Q.; Li, Y. PtM (M= Cu, Co, Ni, Fe) Nanocrystals: From Small Nanoparticles to Wormlike Nanowires by Oriented Attachment. *Chem.—Eur. J.* **2013**, *19*, 233−239.
(36) Erini, N.; Loukrakpam, R.; Petkov, V.; Baranova, E. A.; Yang, R.; Teschner, D.; Huang, Y.; Brankovic, S. R.; Strasser, P. Ethanol Electro-Oxidation on Ternary Platinum-Rhodium-Tin Nanocatalysts: Insights in the Atomic 3D Structure of the Active Catalytic Phase. *ACS Catal.* **2014**, *4*, 1859−1867.
(37) Papadimitriou, S.; Armyanov, S.; Valova, E.; Hubin, A.; Steenhaut, O.; Pavlidou, E.; Kokkinidis, G.; Sotiropoulos, S. Methanol Oxidation at Pt-Cu, Pt-Ni, and Pt-Co Electrode Coatings Prepared by a Galvanic Replacement Process. *J. Phys. Chem. C* **2010**, *114*, 5217−5223.
(38) Beyhan, S.; Coutanceau, C.; Léger, J.-M.; Napporn, T. W.; Kadırgan, F. Promising Anode Candidates for Direct Ethanol Fuel Cell: Carbon Supported PtSn-based Trimetallic Catalysts Prepared by Bönnemann Method. *Int. J. Hydrogen Energy* **2013**, *38*, 6830−6841.
(39) Qi, Z.; Geng, H.; Wang, X.; Zhao, C.; Ji, H.; Zhang, C.; Xu, J.; Zhang, Z. Novel nanocrystalline PdNi alloy catalyst for methanol and ethanol electro-oxidation in alkaline media. *J. Power Sources* **2011**, *196*, 5823−5928.
(40) Kowal, A.; Gojković, S. L.; Lee, K. S.; Olszewski, P.; Sung, Y. E. Synthesis, Characterization and Electrocatalytic Activity for Ethanol Oxidation of Carbon Supported Pt, Pt-Rh, Pt-SnO_2 and Pt-Rh-SnO_2 Nanoclusters. *Electrochem. Commun.* **2009**, *11*, 724−727.
(41) Li, M.; Kowal, A.; Sasaki, K.; Marinkovic, N.; Su, D.; Korach, E.; Liu, P.; Adzic, R. Ethanol Oxidation on the Ternary Pt-Rh-SnO_2/C Electrocatalysts with Varied Pt:Rh:Sn Ratios. *Electrochim. Acta* **2010**, *55*, 4331−4338.
(42) Huang, X.; Zhao, Z.; Chen, Y.; Chiu, C.-Y.; Ruan, L.; Liu, Y.; Li, M.; Duan, X.; Huang, Y. High Density Catalytic Hot Spots in Ultrafine Wavy Nanowires. *Nano Lett.* **2014**, *14*, 3887−3894.

DOI: 10.1021/acsami.5b04391
ACS Appl. Mater. Interfaces 2015, 7, 15061−15067